SIMULATION MODELS FOR TOKAMAK PLASMAS

UCRL-JC--109895

DE93 002876

A.M. DIMITS, B.I. COHEN
Lawrence Livermore National Laboratory,
Livermore, California, USA

ABSTRACT. Two developments in the nonlinear simulation of tokamak plasmas are described: (A) Simulation algorithms that use quasiballooning coordinates have been implemented in a 3D fluid code and a 3D partially linearized (δf) particle code. In quasiballooning coordinates, one of the coordinate directions is closely aligned with that of the magnetic field, allowing both optimal use of the grid resolution for structures highly elongated along the magnetic field as well as implementation of the correct periodicity conditions with no discontinuities in the toroidal direction. (B) Progress on the implementation of a like-particle collision operator suitable for use in partially linearized particle codes is reported. The binary collision approach is shown to be unusable for this purpose. The algorithm under development is a complete version of the test-particle plus source-field approach that was suggested and partially implemented by Xu and Rosenbluth [1].

1. NONLINEAR SIMULATION OF TOKAMAK TURBULENCE USING QUASIBALLOONING COORDINATES

Many instabilities of interest in tokamak plasmas, such as ion-temperature-gradient-driven (ITG) modes, trapped-electron modes, and pressure-driven MHD modes, are highly elongated along the equilibrium magnetic field, which is generally neither purely toroidal nor poloidal. Nonlinear simulations of such instabilities and the resulting turbulence to date have either ignored the periodicity conditions that the fluctuation fields must satisfy or used coordinates aligned with the poloidal and toroidal directions. The former choice is known from linear theory to give incorrect instability growth rates, while the latter is tremendously wasteful of grid resolution, as can be understood from Figs. . To resolve a structure, some number (of order 1) grid cells must fit entirely inside the structure. Typically, the values of the magnetic rotational transform is of order 1. In Fig. (a), the simulation grid in toroidal-poloidal coordinates is sufficiently fine to resolve the larger of the two structures shown, but not the smaller one. When a transformation is made to "ballooning coordinates," in which

one of the coordinates is exactly aligned with the magnetic field as shown in Fig. (b), a grid with the same number of grid cells becomes able to resolve the smaller of the two structures. As an example, for the ITG instability for present-day tokamak parameters, a reduction in the number of grid cells needed in ballooning coordinates of order *100* compared with the number needed in toroidal-poloidal coordinates can be expected. Ballooning coordinates have the disadvantage that the toroidal-poloidal periodicity conditions are difficult to implement satisfactorily.

Here, we report on nonlinear simulation methods that use "quasiballooning coordinates," in which one of the coordinate directions lies approximately (*not necessarily exactly*) along the magnetic field. A lack of alignment is allowed which has a negligible effect on the resolution [2], but permits the implementation of the correct periodicity conditions via exact offset-periodic meshing of the grid lines at opposite ends of the simulation region [Fig. (c)]. They allow calculations in configuration space where the computation of nonlinear terms is much cheaper than in wavenumber space. Finite-difference and discrete-Fourier methods are both applicable on the radial surfaces. For fluid or Vlasov-fluid type simulations, the reduction in computer time needed per timestep decreases in proportion to or more rapidly than the decrease in the number of grid cells needed. Also, in many cases, the coarse parallel grid automatically filters out physically irrelevant but numerically problematic high-frequency modes, permitting much longer timesteps for explicit timestepping, both in particle and fluid codes.

In this paper, applications to slab geometry are considered. Implementations that take into account the effects of toroidal geometry (other than the periodicity conditions) are underway and will be reported elsewhere.

1.1. Basic Method

Let V, θ, and ζ be radial, poloidal and toroidal straight-field-line coordinates [3], normalized so that their values range from 0 to 1. A suitable coordinate choice (V, χ, ζ), where $\chi \equiv \theta - \hat{\iota}(V)\zeta$. Here $\hat{\iota}(V) \simeq \iota(V)$ where $\iota(V)$ is the magnetic rotational transform. The periodicity conditions that a field ψ must satisfy are

$$\begin{aligned} \psi(V, \chi + 1, \zeta) &= \psi(V, \chi, \zeta), \\ \psi(V, \chi - \hat{\iota}, \zeta + 1) &= \psi(V, \chi, \zeta). \end{aligned}$$

The second of these is the one that causes the complication in ballooning coordinates, where $\hat{\iota}(V) = \iota$. Quasiballooning coordinates can be obtained as follows: The V and

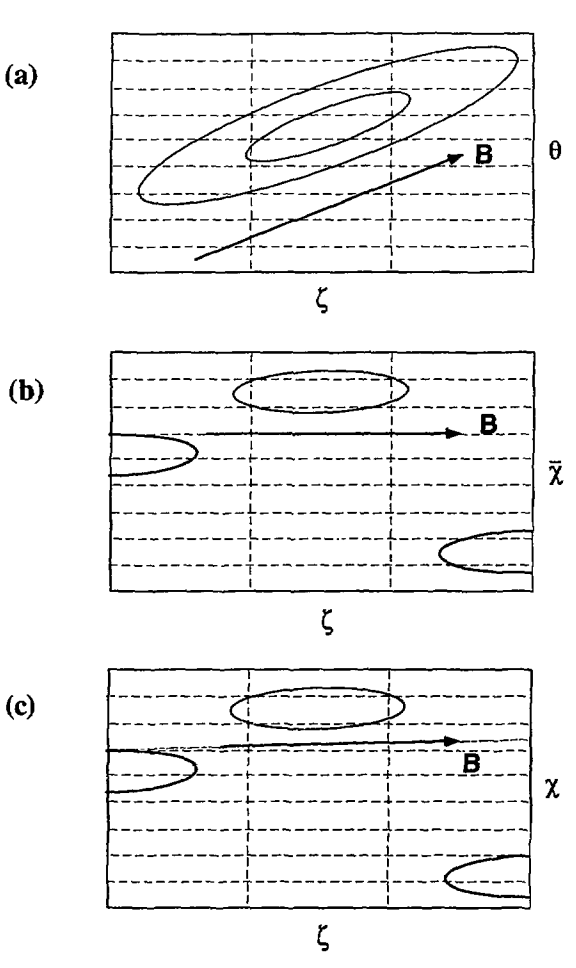

Fig. 1. Grid (dashed lines), magnetic field (arrows), and turbulent structures (ellipses) at a single radial location, as seen in (a) toroidal-poloidal coordinates, (b) ballooning coordinates, and (c) quasiballooning coordinates.

χ coordinates are discretized on a mesh $V_i = (i-1)/N_V$, $\chi_j = (j-1)/N_\chi$, where $i = 1, 2, ..., N_V$, and $j = 1, 2, ..., N_\chi$. At each radial mesh surface $V = V_i$ choose an integer $m(i)$ so as to minimize $\iota(V_i) - \hat{\iota}(i)$, where $\hat{\iota}(i) \equiv m(i)/N_\chi$. The periodicity condition at the $\zeta = 0, 1$ boundary is exactly satisfied by setting $\psi(i, j - m(i), 1) = \psi(i, j, 0)$. The parallel derivative at $V = V_i$ is given by $\nabla_{\|i} = \partial/\partial\zeta + [\iota(V_i) - \hat{\iota}(i)]\partial/\partial\chi$. It is straightforward to show that the resolution lost because $\hat{\iota} \neq \iota$ is negligible. The only restriction on the $\iota(V)$ profiles that can be used is that they be reasonably smooth.

The goal of this work has been to implement quasiballooning coordinates in a fluid code and in a partially-linearized (δf) gyrokinetic particle code. The following issues associated with different implementations have had to be addressed.

1.1.1. Radial Derivatives

It is important that discretizations of the derivative in the physically radial direction be continuous in ζ and obey the correct periodicity conditions at the $\zeta = 0$-1 boundaries [2]. This can be guaranteed by using a discretization of the form

$$[\Delta\psi]_{i,j,k} = \sum_l \alpha_l \hat{\psi}(i + l, \theta[i, j, k], k),$$

where $\hat{\psi}(i + l, \theta[i, j, k], k)$ denotes a value of ψ and $\theta[i, j, k]$ denotes the value of θ at the (V, θ, ζ) index values (i, j, k). Since $\theta = \chi + \hat{\iota}\zeta$, $\theta[i, j, k]$ generally lies between grid lines at radial surface $i + l$ unless $l = 0$. Interpolation between values of ψ at the grid points must therefore be used to determine $\hat{\psi}$. For the resulting difference formula to not have discontinuities in the k index, a spline scheme of at least one order higher than the derivative needed can be used. Alternatively, a Fourier representation in χ provides a natural interpolation scheme with infinite-order accuracy.

1.1.2. Fourier Methods

Discrete-Fourier representations diagonalize many common differential and integral operators and converge more rapidly for smooth fields than finite-difference and finite-element representations. The applicability of standard fast-Fourier transforms for obtaining the discrete Fourier transforms in quasiballooning coordinates is therefore investigated here.

Firstly, the discrete Fourier transform in $\psi(V, \chi, \zeta) \to \psi(V, k_\chi, \zeta)$ can be taken in the same way as for θ since the periodicity conditions on χ are the same as those

on θ. Since the transformation to quasiballooning coordinates alters the periodicity conditions with respect to ζ, and the orientation of the grid with respect to the radial direction, the Fourier transforms with respect to ζ and V are altered. Having made the $\chi \rightarrow k_\chi$ transform, however, the discrete Fourier transforms in the ζ and V directions become accessible. Consider the field $\psi(k_\chi, l)$ where l is the discrete index for $\zeta_l \equiv (l-1)/N_\zeta$, and N_ζ is the number of mesh points in the ζ direction. (The radial variable has been suppressed.) The discrete Fourier transform of $\psi(k_\chi, l)$ is defined by

$$\psi(k_\chi, k_\zeta) \equiv \sum_{l=1}^{MN_\zeta} \psi(k_\chi, l) \exp(-2\pi i k_\zeta l / MN_\zeta),$$

where M is the number of passages made by a χ =const. grid line in the ζ direction before it loops back on itself. Using the "periodicity" condition $\psi(k_\chi, l + N_\zeta) = \exp(2\pi i k_\chi \hat{\iota}) \psi(k_\chi, l)$, it follows that

$$\psi(k_\chi, k_\zeta) \;=\; M \sum_{\xi=1}^{N_\zeta} \exp(-2\pi i m \xi / N_\chi) [\exp(-2\pi i k_\chi \hat{\iota} \xi / N_\chi) \psi(k_\chi, \xi)],$$

where the allowed values of k_ζ are given by $k_\zeta = (MN_\zeta / N_\chi)(m + k_\chi \hat{\iota})$. Note that MN_ζ / N_χ is an integer that represents the number of passages made by a χ =const. grid line in the χ direction before it loops back on itself.

Discrete Fourier transforms can be used in the radial (V) direction, provided that the field being transformed is either bounded or periodic in V (in variables V, θ, and ζ). This is done by multiplying $\psi(k_\chi, l)$ by a phase factor that represents a transformation from χ to θ, so that a radial Fourier transform becomes a sum of fields evaluated at the same θ. Differential and integral operators that are simple in (k_v, k_χ) space can then be applied before transforming back from k_V to V and multiplying by a $\theta \rightarrow \chi$ phase factor.

1.1.3. Periodicity condition on particles

The simulation particles must obey a periodicity condition analogous to that on the fields. Since, however, the radial location of the particles is not restricted to the radial grid surfaces, this periodicity condition must be defined for all radial locations. This can be done by defining a function $\hat{\iota}(V)$ for all V by interpolation (linear or higher-order) between values of $\hat{\iota}(i)$ (already defined) on the radial surfaces $V = V_i$. The particle periodicity condition is then specified by $V(\zeta = 1_-) \leftrightarrow V(\zeta = 0_+)$,

$\chi(\zeta = 1_-) \leftrightarrow \chi(\zeta = 0_+) - \hat{\imath}(V)$, and $\hat{\imath}(V)$ can also be used to prescribe the method for calculating parallel derivatives of the fields at any particle location.

1.1.4. Solution of the gyrokinetic Poisson (quasineutrality) equation

The integral operator in the gyrokinetic quasineutrality equation [4] that is used to solve for the electrostatic potential ϕ is diagonal only when operating on fields that have been Fourier transformed in the poloidal and physically radial directions. The quasineutrality equation then becomes (in suitable normalized variables [4])

$$[\Gamma_0(b) - 1]\phi(\boldsymbol{k}) \simeq -(\overline{n}_\mathrm{i} - n_\mathrm{e}), \tag{1}$$

where $b \equiv k_\perp^2 \rho_\mathrm{i}^2$. If it is desired to use a finite-difference or other non-Fourier representation for the radial direction, then some method for approximating this operator is needed. The use of the first-order-in-b Taylor expansion of $\Gamma_0(b)$ is accurate only in the drift-kinetic limit.

The first-order Pade' approximant for $\Gamma_0(b) \simeq 1/(1+b)$ is an excellent fit for $0 \leq b \lesssim 9$ [5], and is therefore valid well into the gyrokinetic regime. Making this replacement in Eq.(1) gives

$$\begin{aligned} \phi &= \psi + \overline{n}_\mathrm{i} - n_\mathrm{e}, \\ \psi &= (\overline{n}_\mathrm{i} - n_\mathrm{e})/b. \end{aligned}$$

These equations are easily cast into a finite-difference representation by interpreting the division by b as the inversion of a Laplacian. Similarly, for adiabatic electrons, with $\phi = n_\mathrm{e}$, Eq.(1) can be manipulated into the form

$$\begin{aligned} \phi &= \psi + \overline{n}_\mathrm{i}, \\ \psi &= \overline{n}_\mathrm{i}/[2(2b+1)], \end{aligned}$$

which again involves the inversion of an easily-discretized elliptic operator.

1.1.5. Spatial filtering, deposition, and interpolation

Spatial filtering, charge deposition, and field interpolation can be done using variants of the standard procedures using shape factors whose support is a small finite number of grid cell lengths in each direction [6]. In order not to destroy the favorable properties of quasiballooning coordinates, the shape factors must have (a) a physical

shape [i.e., their shape in (V, θ, ζ)] that does not change discontinuously as ζ varies, and (b) an elongation direction close to that of the magnetic field.

For our gyrokinetic particle code, the shape factors for the deposition and interpolation have been chosen to be separable $W(\boldsymbol{x}_\mathrm{p}, \boldsymbol{x}_\mathrm{g}) = W_V(\Delta V) W_\zeta(\Delta\zeta) W_\theta(\boldsymbol{x}_\mathrm{p}, \boldsymbol{x}_\mathrm{g})$, where $W_\theta(\boldsymbol{x}_\mathrm{p}, \boldsymbol{x}_\mathrm{g}) = \hat{W}(\Delta\theta)$ if the magnetic field is in the toroidal direction. Here $\boldsymbol{x}_\mathrm{p} = (V_\mathrm{p}, \theta_\mathrm{p}, \zeta_\mathrm{p})$ is the particle position $\boldsymbol{x}_\mathrm{g} = (V_\mathrm{g}, \theta_\mathrm{g}, \zeta_\mathrm{g})$ is the position of the grid point, $\Delta V \equiv V_\mathrm{g} - V_\mathrm{p}$, and $\Delta\theta$ and $\Delta\zeta$ are defined analogously. In order that the elongation be along the field direction, the argument of W_θ is chosen to represent a poloidal displacement between the particle center and the grid point. The result is that W_θ is a function of $\chi_\mathrm{g} - \chi_\mathrm{p} + [\hat{\iota}(V_\mathrm{g}) - \hat{\iota}(V_\mathrm{p})]\zeta$, where $\zeta = \zeta_\mathrm{g}$ or ζ_p.

The same considerations apply to smoothing, except that $\boldsymbol{x}_\mathrm{p}$ is replaced by a second grid point. Another option for spatial filtering is to use an elliptic field solver based on the difference formulas discussed above. A field ψ can have components at scales smaller than a in direction ζ filtered out to produce a field $\overline{\psi}$ by solving $(1 - a^2\nabla_\zeta^2)\overline{\psi} = \psi$. A faster asymptotic fall off at short wavelengths can be obtained by multiple application of the smoothing algorithm. This applies both to convolutions with shape factors of finite size and to the use of an elliptic solver. A near-Gaussian shape factor can be obtained, for example, by using the fact that $(1 + k^2a^2/n)^n \to \exp(-k^2a^2)$ as $n \to \infty$.

1.2. Fluid Example: Long-Wavelength ITG Turbulence

The results of an implementation of the above methods in a three-dimensional finite-difference nonlinear fluid code are now described.

The following model fluid equations for long-wavelength ITG turbulence in a sheared-slab geometry are used. They are a simplified version of a model used previously [7]. The spatial variables are renamed here as $(V, \theta, \zeta) \to (x, y, z)$, and $\chi \to y'$, and the normalizations are explained in Ref. [7].

$$\begin{aligned}
\frac{\partial\phi}{\partial t} + \frac{1}{\eta_i}\frac{\partial\phi}{\partial y} &= -\alpha\nabla_\parallel v_\parallel + \boldsymbol{\nabla}_\perp \cdot \boldsymbol{D} \cdot \boldsymbol{\nabla}_\perp\phi + \alpha^2 D_\parallel \nabla_\parallel^2\phi, \\
\frac{\partial v_\parallel}{\partial t} + \boldsymbol{v}_{EB} \cdot \boldsymbol{\nabla}_\perp v_\parallel &= -\alpha\nabla_\parallel(T + 2\phi) + \boldsymbol{\nabla}_\perp \cdot \boldsymbol{\mu} \cdot \boldsymbol{\nabla}_\perp\phi + \alpha^2\mu_\parallel\nabla_\parallel^2\phi, \\
\frac{\partial T}{\partial t} + \boldsymbol{v}_{EB} \cdot \boldsymbol{\nabla}_\perp T &= -\frac{\partial\phi}{\partial y} - (\Gamma - 1)\alpha\nabla_\parallel v_\parallel + \boldsymbol{\nabla}_\perp \cdot \boldsymbol{\kappa} \cdot \boldsymbol{\nabla}_\perp\phi + \alpha^2\kappa_\parallel\nabla_\parallel^2\phi,
\end{aligned}$$

where

$$\boldsymbol{v}_{EB} \equiv -\boldsymbol{\nabla}_\perp\phi \times \hat{\boldsymbol{z}},$$

$$\nabla_{\|} \equiv \frac{\partial}{\partial z} + \frac{x}{L_s}\frac{\partial}{\partial y},$$
$$\alpha \equiv \frac{L_T}{\rho_i}\frac{r}{R}.$$

These equations are solved using a three-dimensional explicit finite-difference fluid code which is bounded in the radial (x) direction and periodic in the y and z directions. Heat flow is driven in the steady state by smoothly T and $v_{\|}$ with a damping coefficient that has a finite value γ_0 at the radial boundaries $x = 0$ and 1, and goes smoothly to zero at a finite distance $a \lesssim 0.3$ from the walls.

The $\boldsymbol{E} \times \boldsymbol{B}$ advection nonlinearity has the important simplifying property that its form is unaltered by the transformation to quasiballooning coordinates, i.e.,

$$\frac{\partial\phi}{\partial x}\frac{\partial}{\partial y} - \frac{\partial\phi}{\partial y}\frac{\partial}{\partial x} = \frac{\partial\phi}{\partial x'}\frac{\partial}{\partial y'} - \frac{\partial\phi}{\partial y'}\frac{\partial}{\partial x'}.$$

All results were for $\kappa = \mu = D$, $D_x = 0.02$, $D_y = 0.008$, $D_{\|} = 0.002$, $\eta_i = \infty$, and $\alpha = 5$. The number of grid cells in the x and y directions was $N_x \times N_y = 31 \times 131$. As a starting point, a computation was done with $\iota = 0$, and $N_z = 29$. For this case, the toroidal-poloidal coordinates and the quasiballooning coordinates are identical. The instability grows to a nonlinearly saturated state with partial (not complete) quasilinear relaxation of the temperature profile and a finite heat flux that is carried through the system by the turbulence. The temperature contours show nonlinear structures that are highly elongated in the z direction, i.e., along the magnetic field. When a run with the same parameter values, except $\iota \sim O(1)$ is attempted in toroidal-poloidal coordinates, no instability or turbulence is observed; because of inadequate toroidal resolution, there are no linearly unstable modes. The same case, computed using quasiballooning coordinates results in a robust instability and transport levels similar to the $\iota = 0$ case. Figure shows results from such a run with $q = (1 + \sqrt{5})/2$.

The advantage of quasiballooning coordinates is seen dramatically in the scaling of the number of grid cells needed with α. For the present demonstration simulations, the moderate value $\alpha = 5$ has been chosen. Even for this value, far fewer grid cells are needed in quasiballooning coordinates than in toroidal-poloidal coordinates. In actual experiments, α is typically of order 10 to 100. The number of structures per box length in the y direction increases in direct proportion to α [7]. In toroidal-poloidal coordinates, unless the magnetic field is purely in the toroidal direction, the number of grid cells needed in the toroidal direction is proportional to α, so the

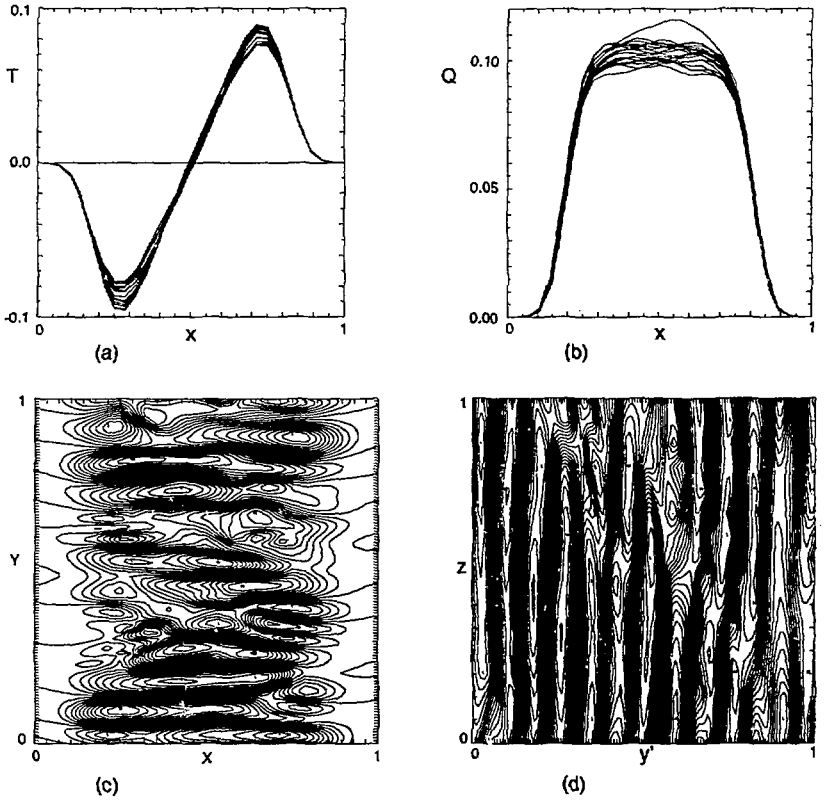

Fig. 2. (a) Profiles of the quasilinear component of $\tilde{T}$ averaged over y and z, and over time intervals of $\Delta t = 0.1$, (b) Profiles of heat flux averaged as in (a), (c) $\tilde{T}$ contours in a x-y cut at $t = 6$, and (d) $\tilde{T}$ contours in a y-z cut at $t = 6$, from a fluid ITG simulation using quasiballooning coordinates with $\iota = (\sqrt{5} - 1)/2$, and $N_x = 29$, and other parameters as stated in the text.

total number of grid cells needed at each radial surface scales as α^2. The number of structures per period in the parallel direction, and therefore the number of grid cells needed in the quasiparallel direction in quasiballooning coordinates, however, is roughly independent of α, so that the total number of grid cells needed per radial surface scales as α.

In the presence of magnetic shear, a similar scaling holds. In addition to the coordinate systems so far discussed, one can define a set of nontwisted "locally quasiballooning" (LQB) coordinates that has $\hat{\iota}(V) \simeq \iota(V_0)$ where V_0 is some radial location at which the coordinates and field are aligned. The difference between results of using quasiballooning coordinates and LQB coordinates increases with increasing shear strength. This difference is a direct result of inadequate resolution away from the magnetic surface when toroidal-poloidal coordinates are used. The number of grid cells needed in LQB coordinates is greater than that needed in quasiballooning coordinates by a factor equal to the radial extent of the simulation region divided by the radial extent of the locally-unstable region of a single toroidal Fourier mode. This factor must be large in order for the simulation to be able to address the presence of structures of large radial extent that are potentially the most dangerous for transport.

1.4. Gyrokinetic Particle Simulation

Slab-ITG instability test runs of the partially-linearized gyrokinetic particle code have been made, both in the linear and nonlinear regime. The linear growth rates and mode structures of the dominant linear eigenmodes in a sheared magnetic field are in agreement with those obtained with standard-coordinate versions of the gyrokinetic code. Figure shows the linear growth of the $(k_y, k_z) = (1, 0)$ mode from a simulation with $\eta_i \equiv L_n/L_T = \infty$, $L_x = L_y = 32\rho_s$, $L_z = 0.5L_yL_T/\rho_s$, $T_e = T_i$, and $L_s = 40L_T$. The time is in units of L_T/c_s. Note that because of the scale invariance of the partially-linearized system, the results are valid for any small value of ρ/L_T.

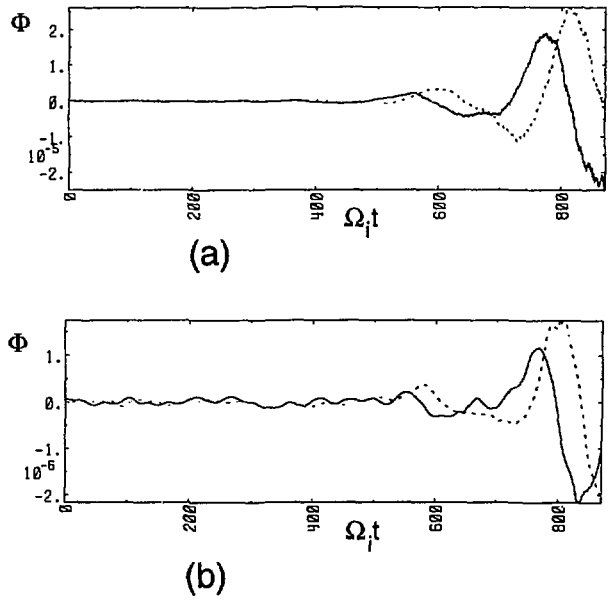

Fig. 3. Real (solid) and imaginary (dotted) parts of ϕ for the $(k_y, k_z) = (1, 0)$ mode at $x/\rho_i = 0.28$ mode from a gyrokinetic run using (a) quasiballooning coordinates and (b) toroidal-poloidal coordinates, with $\eta_i = \infty$, $L_x = L_y = 32\rho_s$, $L_z = 0.5 L_y L_T/\rho_s$, $T_e = T_i$, and $L_s = 40 L_T$.

2. COLLISION OPERATORS FOR PARTIALLY-LINEARIZED PARTICLE SIMULATION CODES

Standard and partially-linearized particle simulation algorithms, in their basic form, are essentially collisionless [6]. Many processes of interest in plasma physics, for which kinetic simulation studies are needed, involve collisions. Our effort is directed to implementing a usable energy- and momentum-conserving, like-particle collision operator in partially-linearized δf gyrokinetic particle codes. For given particle number, such codes have been shown to have tremendously reduced noise compared with standard fully-nonlinear particle simulation codes [8].

While electron collisions off ions can often be modelled as pitch-angle scattering, because of the large ion-electron mass ratio [9,10], for like particle collisions additional steps must be taken to guarantee that the collision model conserves energy and momentum. Two approaches have been used. The first approach [1], the linearized Landau collision operator is separated into test-particle terms which are treated by standard Monte-Carlo methods, and and source-sink field terms that enforce the conservation laws. The second approach [11] is a binary scheme in which the random accelerations and displacements of spatially nearby pairs of particles are correlated so as to exactly conserve the energy and momentum of each pair.

While the formulations of the collision operators are given in their respective contexts in the papers of Xu and Rosenbluth [1] and of Ma, Sydora, and Dawson [11], considerations beyond those addressed there are involved in deciding which approach is to be preferred in our partially-linearized simulations. The binary algorithm of Ref. [11] is formulated for standard fully-nonlinear simulations only, but not for partially-linearized simulations. In the latter, the prescription of Ref. [11] would result in collisions that conserve the energy and momentum of the zero-order or marker particles, but not of the physical first-order (δf) energy and momentum. Xu and Rosenbluth [1] provided an almost complete derivation of, but did not implement, the source and sink terms necessary for energy and momentum conservation. The gyroaverages were formulated in terms of Bessel functions involving the perpendicular Fourier mode numbers. A much more efficient procedure for nonlinear (partially-linearized) simulations is to average over a finite number of points on a circle centered at the gyrocenter [4]. This necessitates a reformulation of source-sink terms in terms of explicit gyroaverages, particle-grid depositions, and field-particle interpolations. Since the deposition and interpolation steps are computationally expensive, it is necessary to consider the implementation in some detail in order to

decide on its feasibility.

2.1. Inapplicability of the Binary Collision Approach

The primary consideration that turns out to decide which approach is to be preferred is the impossibility of implementing a binary operator in a partially-linearized code.

Consider a gas consisting of two particles with initial velocities v_1 and v_2 and weights w_1 and w_2, and formally integrate the perturbed Boltzmann collision operator over a time interval such that one collision occurs with final velocities v_1' and v_2' that can result from v_1 and v_2 by a standard energy- and momentum-conserving collision. The result for the change in the velocity distribution function due to the collision is

$$\delta f(v,t+\tau) - \delta f(v,t) = (w_1+w_2)\{\delta(v-v_1') - \delta(v-v_1) + \delta(v-v_2') - \delta(v-v_2)\}. \tag{2}$$

This result clearly conserves particle number, energy, and momentum. It can be generalized to collisions between many pairs of particles by summing over colliding pairs. The key feature of Eq.(2) is that markers both at the new and old velocities are required to represent the final distribution function. The free parameters made available by the additional marker particles are necessary to permit the collisions both to conserve number, energy, and momentum, and to permit a prescription of the collision rate. This makes the binary algorithm totally unusable for partially-linearized simulations.

2.2. Development of a Test-Particle + Source Algorithm

For the reason explained in the previous subsection, we have developed an implementation based on the approach of Ref. [1]. Our implementation includes the source/sink terms necessary for energy and momentum conservation and is in a form suitable for partially-linearized gyrokinetic particle simulations. The main steps involved are as follows.

The linearized Landau collision operator can be written as [1]

$$C(\delta f) = C_{\rm tp}(\delta f) + p(\delta f)F_{\rm M}, \tag{3a}$$

where

$$C_{\rm tp}(\delta f) = \frac{\partial}{\partial v_\perp^2}[\nu_{s\perp} v^2 \delta f + \frac{1}{2}\frac{\partial}{\partial v_\perp^2}(\nu_\perp v^4 \delta f) + \frac{1}{2}\frac{\partial}{\partial v_\parallel}(\nu_{\parallel\perp} v^3 \delta f)]$$
$$+ \frac{\partial}{\partial v_\parallel}[\nu_{s\parallel} v_\parallel \delta f + \frac{1}{2}\frac{\partial}{\partial v_\parallel}(\nu_\parallel v^2 \delta f) + \frac{\partial}{\partial v_\perp^2}(\nu_{\parallel\perp} v^3 \delta f)]$$
$$+ \frac{1}{v_\perp}\frac{\partial}{\partial \varphi}[\frac{1}{v_\perp}\frac{\partial}{\partial \varphi}(G\delta f)], \tag{3b}$$

and

$$p(\delta f) = \frac{1}{n_0 v_T^2}\left(\boldsymbol{v}\cdot\int d\boldsymbol{v}\,\boldsymbol{v} F \delta f + \frac{2}{3}\int d\boldsymbol{v}(v^2 F - 3G - H)\delta f\right), \tag{3c}$$

where $\nu_{s\parallel}$, $\nu_{s\perp}$, $\nu_\parallel$, $\nu_{\parallel\perp}$, F, G, and H are functions of $v_\parallel$ and $v_\perp$ defined in Ref. [1]. First, δf is expressed in terms of the gyroaveraged distribution function g, accurate to first order in the gyrokinetic smallness parameter [13], via

$$\delta f = h - \frac{q}{T} F_{\rm M} \phi, \tag{4a}$$

where

$$h = g + \frac{q}{T} F_{\rm M} \overline{\phi}, \tag{4b}$$

where $\overline{\phi}$ is the gyroaveraged potential. Next, the spatial position is expressed in terms of the lowest-order gyrocenter position, $\boldsymbol{R} \equiv \boldsymbol{x} - \boldsymbol{\rho}$, where $\rho \equiv \hat{\boldsymbol{b}} \times \boldsymbol{v}/\Omega$. This requires the following transformation formulas for the partial derivatives:

$$\left.\frac{\partial}{\partial v_\perp^2}\right|_x = \left.\frac{\partial}{\partial v_\perp^2}\right|_R - \frac{\boldsymbol{\rho}}{2v_\perp^2}\cdot\frac{\partial}{\partial \boldsymbol{R}},$$
$$\left.\frac{\partial}{\partial \varphi}\right|_x = \left.\frac{\partial}{\partial \varphi}\right|_R - \boldsymbol{\rho}\times\hat{\boldsymbol{b}}\cdot\frac{\partial}{\partial \boldsymbol{R}}.$$

Finally, the collision operator is gyroaveraged, i.e., averaged with respect to φ with $\boldsymbol{R}$ held fixed. The results are

$$\langle C_{\rm tp}(g)\rangle = \frac{\partial}{\partial v_\perp^2}(\nu_{s\perp} v^2 g) + \frac{\partial}{\partial v_\parallel}(\nu_{s\parallel} v_\parallel g) + \frac{1}{2}\frac{\partial^2}{\partial (v_\perp^2)^2}(\nu_\perp v^4 g)$$
$$+ \frac{1}{2}\frac{\partial^2}{\partial v_\parallel^2}(\nu_\parallel v^2 g) + \frac{\partial^2}{\partial v_\perp^2 \partial v_\parallel}(\nu_{\parallel\perp} v^3 g)$$
$$+ \frac{1}{2v_\perp^2}\rho^2 \nabla_R^2\left[\left(\frac{v^4\nu_\perp}{8v_\perp^2} + G\right)g\right], \tag{5a}$$

$$\langle C_{\rm tp}(F_{\rm M}\overline{\phi})\rangle = F_{\rm M}\left[-v^2(\nu_{s\perp} + \nu_\perp\frac{v^2}{2v_\perp^2})\frac{\partial\overline{\phi}}{\partial v_\perp^2} + \left(\frac{v^4\nu_\perp}{4v_\perp^4} + \frac{G}{v_\perp^2}\right)\rho^2\nabla_R^2\overline{\phi}\right], \tag{5b}$$

$$\langle C(F_{\rm M}\phi)\rangle = 0, \tag{5c}$$

where $\partial/\partial v_\perp^2$ is now evaluated at fixed $\boldsymbol{R}$. In addition, the gyroaveraging of the p term is trivial since the nonvanishing piece $p(g + qF_M\overline{\phi}/T)$ depends only on gyroaveraged quantities.

All of the resulting terms can be interpreted as either test-gyrocenter terms or as sources that can be evaluated by standard deposition, interpolation, and ring averaging [4]. This operator has been implemented in a two-dimensional partially-linearized gyrokinetic code. The test-particle portion of the operator has been previously tested [14]. Two kinds of tests of the source terms are presently underway: (A) Marker particles is loaded from a uniform Maxwellian. A direction in phase space is chosen, depending on which conservation law is to be tested. The weights of the particles are initialized to be one in a narrow interval about a single value of the chosen phase space coordinate, and zero outside this interval, and independent of the other phase space directions. If it were not for the source-sink terms, the zero-order drag and diffusion acting on those particles would cause the value of the first-order moment associated with the chosen phase space direction to evolve. When the source terms are taken into account, however, the evolution of the moment should be small. (B) Tests of the scaling of the damping rate of ion acoustic waves in the collisional fluid regime provide a sensitive test of the parallel momentum conservation. Initial indications are that particle number, (canonical) momentum, and energy are well conserved for sufficient particle density, although further tests are still being undertaken. These simulation runs indicate a relative slowdown of the particle code by roughly a factor of 2 on the Cray-2, when the collisions are applied each timestep. The slowdown is due primarily to the deposition and interpolation steps involved in computing the conserving source-sink fields. A more typical circumstance for applications will be to execute the collision package much less often than at every time step because the ion-ion collision frequency is usually much less than the diamagnetic drift frequencies of interest. If the plasma is much more collisional, the particle-code calculations become more expensive and a a fluid approach becomes more appropriate on physical grounds.

3. CONCLUSIONS

Quasiballooning coordinates are coordinates that are nearly aligned with the equilibrium magnetic field. They permit the construction of grids that optimally resolve structures that are elongated along the magnetic field and that satisfy the correct physical periodicity conditions, even in the presence of magnetic shear. They have

been implemented in a fluid code and in a partially-linearized gyrokinetic particle code. Results from applications of these codes to ITG turbulence are encouraging.

A like-particle collision operator that correctly conserves particle number, momentum and energy, and is suitable for use in partially linearized particle codes has been developed and implemented. The algorithm is a complete version of the test-particle plus source-field approach that was suggested and partially implemented by Xu and Rosenbluth [1]. The binary collision approach was shown to be unusable for this purpose.

ACKNOWLEDGMENTS

The author gratefully acknowledges useful discussions with S. C. Cowley, J. F. Drake, T. J. Williams, T. M. Antonsen Jr., R. H. Cohen, and L. LoDestro. This work was performed by LLNL for USDoE under contract W-7405-ENG-48.

References

[1] X.Q. Xu and M.N. Rosenbluth, Phys. Fluids *B3*, 627 (*1991*).

[2] A.M. Dimits in the Proceedings of the *14th. International Conference on the Numerical Simulation of Plasmas*, (SAIC-NRL, Annapolis, MD 1991, paper PWA5.

[3] S. Hamada, Nucl. Fusion **2**, 23 (1962).

[4] W. W. Lee, J. Comp. Phys. **72**, 243 (1987).

[5] W. Dorland, G.W. Hammett, Liu Chen, W. Park, S.C. Cowley,, S. Hamaguchi, and W. Horton, Bull. APS **35**, 2005 (1990, paper 4R10).

[6] C. K. Birdsall and A. B. Langdon, *Plasma Physics via Computer Simulation* (1985, McGraw-Hill, New York),

[7] J.F. Drake, P.N. Guzdar, and A.M. Dimits, Phys. Fluids B**3**, 1937 (1991).

[8] M. Kotschenreuther, Bull. Am. Phys. Soc. **34**, 2107 (1988); Proceedings of the *14th. International Conference on the Numerical Simulation of Plasmas*, (SAIC-NRL, Annapolis, MD 1991, paper PT20).

[9] R. Shanny, J.M. Dawson, and J.M. Greene, Phys. Fluids **10**, 1281 (1967).

[10] A. Boozer and G. Kuo-Petravic, Phys. Fluids **24**, 851 (1981).

[11] S. Ma, R. D. Sydora, and J. M. Dawson, UCLA-IPFR Report PPG-1371 (August, 1991).

[12] A.M. Dimits, PhD. Thesis, Princeton University, Feb. 1988.

[13] W.W. Lee, Phys. Fluids **26**, 556 (1983).

[14] T.D. Rognlien and T.A. Cutler, Nucl. Fusion **20**, 1003 (1980).